PIER C

(Received 7 December 2025, Accepted 9 January 2026, Scheduled 6 March 2026)

Optimized Hierarchical Nested Array for Enhanced Uniform Degrees of Freedom in Sparse Array DOA Estimation

Guibao Wang[1, *], Keyi Yu[1], Xianghui Wang[1], and Shuzhen Wang[2, 3]

[1] *School of Electronic Information and Artificial Intelligence*
Shaanxi University of Science & Technology, Shanxi 710021, China
[2] *School of Computer Science and Technology, Xidian University, Xi'an 710071, China*
[3] *Shaanxi Lingyaohei Technology Co., Ltd, Xi'an 712046, China*

ABSTRACT: Sparse arrays have been extensively investigated for their capability to enhance degrees of freedom (DOFs). However, a conventional nested array configuration is susceptible to strong mutual coupling (MC), while its achievable uniform DOFs (uDOFs) remains limited. To address these challenges, this paper proposes two optimized hierarchical nested arrays, designated as OHNA-I and OHNA-II. OHNA-I reconstructs the spatial arrangement of subarrays through a hierarchical shifting operation, effectively extending the continuous segment of the difference co-array (DCA). Building on this, OHNA-II further optimizes the subarray geometry via sensor displacement, achieving a better balance between uDOF enhancement and MC suppression, thereby maintaining higher uDOFs while reducing inter-sensor coupling interference. Numerical simulation results demonstrate that, under the same number of physical sensors, the proposed structures — particularly OHNA-II — achieve a greater number of uDOFs than existing classical sparse arrays. Furthermore, in scenarios with strong MC, the proposed structure exhibits superior robustness and lower root mean square error (RMSE) in DOA estimation.

1. INTRODUCTION

Array signal processing is utilized across multiple fields, such as navigation [1], wireless networks [2], and radar [3]. Recent advances in sparse array design offer high-resolution direction of arrival (DOA) estimation with reduced hardware complexity. Early foundational designs include minimum redundancy arrays (MRAs) [4], nested arrays (NAs) [5], and coprime arrays (CAs) [6] which leverage difference co-array (DCA) to enhance uDOFs, improving source resolution capability.

A compression factor is utilized in a coprime array with displaced subarrays (CADiS) [7] to increase sensor spacing. In [8], a thinned coprime array (TCA) achieves sensor redundancy reduction while maintaining uDOFs comparable to conventional CA. In [9], the extended padded coprime array (ePCA) incorporate hole-filled subarrays to extend continuous co-array segments, enhancing uDOFs and mitigating MC.

The DOA estimation accuracy in coprime arrays is limited by co-array holes and restricted uDOFs. To address this, researchers combined NA and CADiS features to develop NA-CADiS [7], maintaining high uDOFs while minimizing virtual array holes via sparse optimization. In [10], the augmented nested arrays (ANAs) improve uDOFs and reduce redundancy through subarray optimization (ANAI-1) and MC suppression (ANAI-2), though both demand precise sensor placement. In [11], dilated nested arrays (DNAs) further enhance uDOFs while reducing coupling. In [12], a nested array with three sub-ULAs (NA-TS) reconfigures NA geometry to moderately improve both uDOFs and coupling. In [13], generalized augmented multi-subarray nested arrays (GAMSNAs) are proposed, which enhance uDOFs through uniform subarray reconfiguration, and the latter mitigates coupling better but offers limited uDOF gain.

Therefore, this paper focuses on enhancing DOA estimation performance by maximizing uDOFs and mitigating MC. The key contributions are outlined below:

- OHNA configurations are proposed based on a shifting operation. Extensive simulation experiments demonstrate that these configurations significantly enhance uDOFs, with OHNA-II effectively mitigating MC.
- By reconfiguring the positional relationship between dense and sparse subarrays in the nested array, OHNA-I increases the uDOFs of the virtual difference co-array while maintaining a simple and implementable structure.
- OHNA-II improves overall performance by optimizing both the geometry and sensor placement, thereby extending uDOFs and reducing MC.

Following the introduction, Section 2 revisits signal model and array configuration. Section 3 outlines research motivation and introduces the proposed OHNA configurations. Section 4 presents numerical simulations for performance evaluation. Section 5 provides the concluding remarks of this work and outlines potential directions.

Notations In this paper, uppercase bold letters and lowercase bold letters represent matrices and vectors, respectively.

---

* Corresponding author: Guibao Wang (gbwang@sust.edu.cn).

doi:10.2528/PIERC25120702

Published by THE ELECTROMAGNETIC ACADEMY

The superscripts $(\cdot)^*$, $(\cdot)^H$, and $(\cdot)^T$ denote complex conjugate, Hermitian transpose, and transpose, respectively. $\mathbb{E}(\cdot)$ is the statistical expectation operator. $vec(\mathbf{A})$ represents the vectorization of matrix $\mathbf{A}$. The symbol $\otimes$ denotes the Kronecker product, and the symbol $\circ$ denotes the Khatri-Rao product. $\langle a, b\rangle$ denotes integer set $\{x \in \mathbb{Z} | a \leq x \leq b\}$. $\|\cdot\|_F$ represents the Frobenius norm of a matrix. card $\{\cdot\}$ denotes the cardinality, and diag$(\cdot)$ denotes a diagonal matrix.

2. PRELIMINARIES

2.1. Signal Model

Consider Q narrowband signals with directions of arrival $\Theta = [\theta_1, \theta_2 ..., \theta_Q]$. These signals are received by a sparse array consisting of N sensors, whose positions are given by

$$\mathbb{S} = \{b_l d | b_l \in \mathbb{Z},\, b \in \langle 0, N-1\rangle\} \tag{1}$$

where the inter-sensor spacing d is $\lambda/2$.

Without considering MC, the received signal at moment t is expressed as

$$\mathbf{x}(t) = \mathbf{A}\mathbf{s}(t) + \mathbf{n}(t) \tag{2}$$

where $\mathbf{s}(t) = [s_1(t), s_2(t), ..., s_Q(t)]^T$ is the signal vector; $\mathbf{A} = [\mathbf{a}(\theta_1), \mathbf{a}(\theta_2), ..., \mathbf{a}(\theta_Q)]$ is the manifold matrix with $\mathbf{a}(\theta_q) = \left[1, e^{-j2\pi b_1 d \sin(\theta_q)/\lambda}, ..., e^{-j2\pi b_{N-1} d \sin(\theta_q)/\lambda}\right]^T$, and noise vector $\mathbf{n}(t) \sim \mathcal{CN}(0, \sigma_n^2 \mathbf{I}_N)$. The covariance matrix is expressed as

$$\hat{\mathbf{R}}_{\mathbf{x}} = \mathbb{E}\left[\mathbf{x}(t)\mathbf{x}^H(t)\right] = \mathbf{A}\mathbf{R}_{\mathbf{S}}\mathbf{A}^H + \sigma_n^2 \mathbf{I}_N \tag{3}$$

where $\mathbf{R}_{\mathbf{S}} = \text{diag}([\sigma_1^2, \cdots, \sigma_q^2, \cdots, \sigma_Q^2])$ is the source covariance matrix, and σ_q^2 is the signal power.

Definition 1: The DCA $\mathbb{D}$ is formulated as

$$\mathbb{D} = \{b_i - b_j | b_i, b_j \in \mathbb{S}\} \tag{4}$$

Definition 2: Let $\mathbb{P}$ denote the longest continuous segment in DCA, and the number of uDOFs is given by the cardinality of $\mathbb{P}$, i.e., $\mathbb{U} = \text{uDOFs}(\mathbb{S}) = \text{card}\{\mathbb{P}\}$.

2.2. Mutual Coupling

When the MC between adjacent sensors is taken into account, the signal model is formulated as [14, 15]

$$\mathbf{x}(t) = \mathbf{C}\mathbf{A}\mathbf{s}(t) + \mathbf{n}(t) \tag{5}$$

For linear arrays, the mutual coupling matrix is commonly approximated by a B-banded symmetric Toeplitz matrix, expressed as

$$[\mathbf{C}]_{b_i, b_j} = \begin{cases} m_{|b_i - b_j|}, & |b_i - b_j| \leq B \\ 0, & \text{otherwise} \end{cases} \tag{6}$$

where the coupling coefficient is $m_a = m_1 e^{-j(\rho-1)\pi/8}/\rho\ (2 \leq \rho \leq B)$ [16]. B is the scope of coupling, which satisfies the condition $1 = m_0 > |m_1| > \cdots > |m_B| > 0$. Although MC generally decays with increasing sensor spacing in practical scenarios, we set the effective bandwidth to $B = 100$. This parameter is chosen to simulate an extreme mutual coupling environment where coupling effects remain significant across the entire array aperture. The purpose of this stringent setting is to thoroughly validate the robustness of the proposed array configuration under strong interference through rigorous stress testing, thereby clearly demonstrating its performance advantage [17, 18].

Definition 3: The weight function for a virtual array quantifies the distribution of sensor pairs across time delays in the DCA, that is,

$$w(\gamma) = \left\{(\eta_i, \eta_j) \in \mathbb{S}^2 | \eta_i - \eta_j = \gamma,\, \gamma \in \mathbb{D}\right\} \tag{7}$$

where $\mathbb{S}^2$ represents the set of all possible pairs of sensor positions, and η_i and η_j are both selected from the set $\mathbb{S}$.

The weight function $w(\gamma)$ for a linear array consisting of N sensors possesses the following properties [19]

$$w(0) = N, \quad \sum_{\gamma \in \mathbb{D}} w(\gamma) = N^2, \quad w(\gamma) = w(-\gamma) \tag{8}$$

The first three weight functions, $w(1)$, $w(2)$, and $w(3)$, exert the most significant mutual coupling effects on the array [17]. Hence, achieving smaller values for $w(1)$, $w(2)$, and $w(3)$ is a key objective for sparse arrays.

Definition 4: For a sparse array with a fixed array aperture, the MC effect is quantified as [20]

$$\mathcal{L}(R) = \frac{\|\mathbf{C} - \text{diag}\{\mathbf{C}\}\|_F}{\|\mathbf{C}\|_F} \tag{9}$$

2.3. Nested Array (NA)

The NA with a total of $N = M_1 + M_2$ physical sensors can reach $2M_2(M_1 + 1) - 1$ DOFs, and the sensor positions are arranged as follows

$$S = \{0, d, ..., M_1 d, (M_1 + 1)d, ..., M_2(M_1 + 1)d\} \tag{10}$$

Table 1 presents the optimal element allocation for the NA subarray. Consider a two-level NA with 7 sensors and an adjacent sensor spacing of $d = 1$. As illustrated in Figure 1, the DCA is generated from the cross-differences between the first

TABLE 1. Optimal element allocation for NA subarrays.

	Optimum M_1	Optimum M_2
odd	$(N-1)/2$	$(N+1)/2$
even	$N/2$	$N/2$

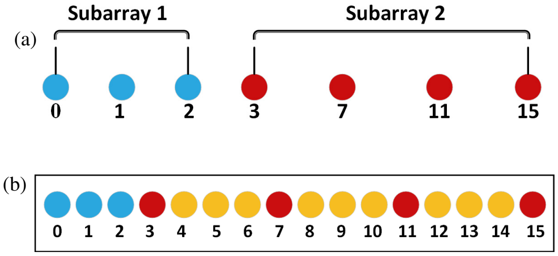

FIGURE 1. A 7-sensor nested array. (a) Sensor positions. (b) Nonnegative difference co-array of NA.

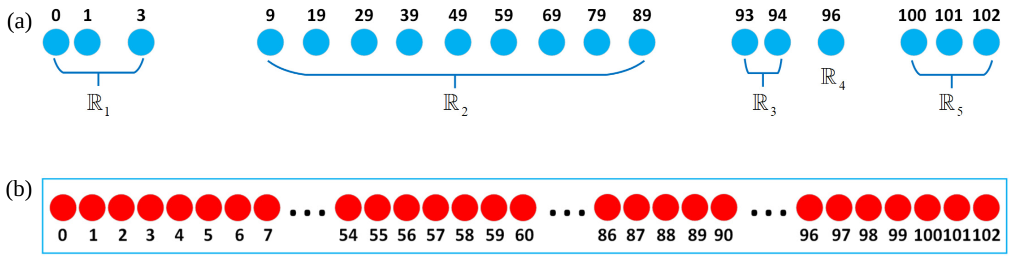

FIGURE 2. OHNA-I configuration comprising 18 sensors. (a) Sensor positions. (b) Nonnegative difference co-array of OHNA-I.

and second subarrays, introducing three virtual sensors at positions $\{4,5,6\}$. They can be viewed as virtual sensors formed by shifting subarray 1 to the right by $4d$, thereby filling the gaps between sensor 3 and sensor 7 in subarray 2. As a result, all remaining gaps are filled, forming a uniform linear array (ULA).

3. OPTIMIZED HIERARCHICAL NESTED ARRAY CONFIGURATION

3.1. Motivation

Optimizing array configuration is pivotal for enhancing DOA estimation performance. Building upon the concept of virtual shifting in NA, this work introduces two improved hierarchical configurations, namely OHNA-I and OHNA-II. OHNA-I reconfigures sensor locations within the subarray to significantly increase the uDOF while maintaining a large array aperture. However, this configuration may introduce severe MC, potentially compromising DOA estimation accuracy, and OHNA-II addresses this limitation by optimizing the geometric configuration and sensor arrangement of OHNA-I. This design effectively mitigates MC while preserving high uDOF, thereby enhancing the robustness and accuracy of DOA estimation.

3.2. OHNA-I

Proposition 2. (OHNA-I Configuration): Let M_1 and M_2 be integers, while $M_1 \geq 8$, $M_2 \geq 8$. The proposed OHNA-I structure is defined by the sensor set

$$\mathbb{R}_{\text{OHNA-I}} = \mathbb{R}_1 \cup \mathbb{R}_2 \cup \mathbb{R}_3 \cup \mathbb{R}_4 \cup \mathbb{R}_5 \tag{11}$$

$$\begin{cases} \mathbb{R}_1 = \{0,1,3\} \\ \mathbb{R}_2 = \{\ell_1(M_1+1)-1 | 1 \leq \ell_1 \leq M_2\} \\ \mathbb{R}_3 = \{M_2(M_1+1)+3+\ell_2 | 0 \leq \ell_2 \leq M_1-8\} \\ \mathbb{R}_4 = M_1M_2+M_1+M_2-3 \\ \mathbb{R}_5 = \{M_1M_2+M_1+M_2+1+\ell_3 | 0 \leq \ell_3 \leq 2\} \end{cases} \tag{12}$$

The sensor positions in sets $\mathbb{R}_1$, $\mathbb{R}_2$, $\mathbb{R}_3$, $\mathbb{R}_4$, and $\mathbb{R}_5$ exhibit nonuniform spacing, which satisfies the requirement for array sparsity. Figure 2 illustrates the OHNA-I configuration with $N = 18$ sensors. Since the virtual DCA corresponding to OHNA-I contains no holes, its non-negative continuous segment spans from 0 to 102, providing OHNA-I with a total of 205 uDOFs.

Proposition 3. OHNA-I is categorized as a restricted type of array furthermore, (a) its difference co-array is continuous over the interval $\langle -v-2, v+2 \rangle$, where $v = (M_1+1)(M_2+1)$, and (b) the overall count of unique DOFs can reach $2v+5$.

Proof: (a) As the DCA of OHNA-I is symmetric, its nonnegative part is the mirror of the negative part. Hence, to simplify the proof, it is sufficient to establish that the nonnegative part of D in definition 1 ensures continuity form 0 to $(M_1+1)(M_2+1)+2$.

The self-difference set of $\mathbb{R}_1$ is $\langle 0,3 \rangle$. The cross-difference sets between $\mathbb{R}_5$ and $\mathbb{R}_3$, and between $\mathbb{R}_5$ and $\mathbb{R}_4$, are $\langle 6, M_1 \rangle$ and $\langle 4,6 \rangle$, respectively. Combining these results, we can derive a continuous set: $\langle 0, M_1 \rangle$.

The cross-difference sets between $\mathbb{R}_2$ and $\mathbb{R}_1, \mathbb{R}_3, \mathbb{R}_4, \mathbb{R}_5$ are given as follows

$$\begin{cases} \mathbb{D}^+_{1,2} = \{\lambda_1(M_1+1)-4, \lambda_1(M_1+1)-2, \\ \qquad \lambda_1(M_1+1)-1 | 1 \leq \lambda_1 \leq M_2\} \\ \mathbb{D}^+_{3,2} = \{\lambda_4(M_1+1)+4, \lambda_4(M_1+1)+M_1-4 \\ \qquad | 1 \leq \lambda_4 \leq M_2-1\} \\ \mathbb{D}^+_{4,2} = \{\lambda_1(M_1+1)-3 | 1 \leq \lambda_1 \leq M_2\} \\ \mathbb{D}^+_{5,2} = \{\lambda_1(M_1+1)+1, \lambda_1(M_1+1)+2, \\ \qquad \lambda_1(M_1+1)+3 | 1 \leq \lambda_1 \leq M_2\} \end{cases} \tag{13}$$

The self-difference set of $\mathbb{R}_2$ is expressed as

$$\mathbb{D}^+_2 = \{\lambda_4(M_1+1) | 1 \leq \lambda_4 \leq M_2-1\} \tag{14}$$

For $\lambda_1 = \lambda_4 = 1$, $\mathbb{D}^+_2$ contains (M_1+1); $\mathbb{D}^+_{3,2}$ contains $\{M_1+5, 2M_1-3\}$; and $\mathbb{D}^+_{5,2}$ covers the range $\langle M_1+2, M_1+4 \rangle$. For $\lambda_1 = \lambda_4 = 2$, $\mathbb{D}^+_{1,2}$ covers $\{2M_1-2, 2M_1, 2M_1+1\}$; $\mathbb{D}^+_{4,2}$ covers $2M_1-1$; and $\mathbb{D}^+_2$ contains $2(M_1+1)$. Therefore, a continuous segment from (M_1+1) to $2(M_1+1)$ is formed. Extending this logic, we can derive the range from (M_1+1) to $M_2(M_1+1)-1$.

The cross-difference sets among $\mathbb{R}_3$, $\mathbb{R}_4$, $\mathbb{R}_5$ and $\mathbb{R}_1$ can be obtained as follows:

$$\begin{cases} \mathbb{D}^+_{3,1} = \{M_2(M_1+1)+\lambda_2 | 0 \leq \lambda_2 \leq M_1-5\} \\ \mathbb{D}^+_{4,1} = \{(M_2+1)(M_1+1)-7, (M_2+1) \\ \qquad (M_1+1)-5, (M_2+1)(M_1+1)-4\} \\ \mathbb{D}^+_{5,1} = \{(M_2+1)(M_1+1)+\lambda_2 | -3 \leq \lambda_2 \leq 2\} \end{cases} \tag{15}$$

According to (15), $\mathbb{D}^+_{3,1}$ covers the range $\langle M_2(M_1+1), M_2(M_1+1)+M_1-5 \rangle$; $\mathbb{D}^+_{4,1}$ contains $\{(M_1+1)(M_2+1)-5, (M_1+1)(M_2+1)-4\}$; $\mathbb{D}^+_{5,1}$ covers the range $\langle (M_2+1)(M_1+1)-3, (M_2+1)(M_1+1)+2 \rangle$, and this proof is finalized.

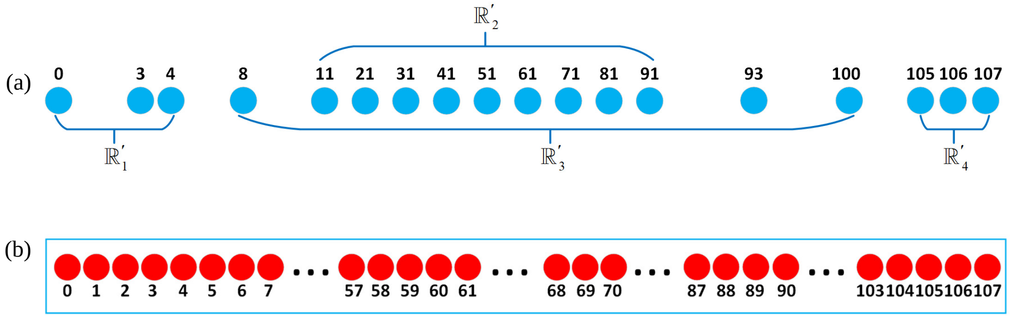

FIGURE 3. OHNA-II configuration with 18 sensors. (a) Sensor positions. (b) Nonnegative difference co-array of OHNA-I.

(b) This property is verified by utilizing the cross-correlation characteristics between self-sensor pairs and cross-sensor pairs within the subarrays of OHNA-I.

According to (a), the virtual DCA of OHNA-I is hole-free, and continuous within the range $\langle -\left(M_1+1\right)\left(M_2+1\right)-2, \left(M_1+1\right)\left(M_2+1\right)+2\rangle$, namely $\langle -v-2, v+2\rangle$. Therefore, the unique uDOFs is $2\left(M_1+1\right)\left(M_2+1\right)+5$, namely $2v+5$.

Proposition 4. For OHNA-I configuration with P sensors, the weight function $w(\gamma)$ $(\gamma=1,2,3)$ is

$$\begin{cases} w(1)=M_1-5, & M_1\geq 8 \\ w(2)=\begin{cases} 3, & M_1=8 \\ M_1-6, & M_1\geq 9 \end{cases} \\ w(3)=\begin{cases} 1, & M_1=8 \\ 2, & M_1=9 \\ M_1-8, & M_1\geq 10 \end{cases} \end{cases} \tag{16}$$

Proof: The values $w(\gamma)(\gamma=1,2,3)$ represent the occurrence counts associated with key values 1, 2, and 3 in the DCA, respectively.

According to the proof of Proposition 3, for $M_1=8$, $\mathbb{D}_1^{+}$ contains the lags $\{1,2,3\}$, while $\mathbb{D}_5^{+}$ contributes $\{1,2\}$, and $\mathbb{D}_{4,3}^{+}$ includes lag 2. Thus, $w(1)=3$, $w(2)=3$, and $w(3)=1$. When $M_1=9$, $\mathbb{D}_1^{+}$ and $\mathbb{D}_{4,3}^{+}$ contain the lags $\{1,2,3\}$, respectively, and $\mathbb{D}_5^{+}$ contains the lags $\{1,2\}$. Additionally, $\mathbb{D}_3^{+}$ includes the key value 1. Hence, $w(1)=4$, $w(2)=3$, and $w(3)=2$. When $M_1=10$, $\gamma=3$ is contributed by $\mathbb{D}_1^{+}$ and $\mathbb{D}_{4,3}^{+}$ and $w(3)=2$. Moreover, $\mathbb{D}_3^{+}$ provides additional lags $\{1,2\}$, leading to $w(1)=5$ and $w(2)=4$. For $M_1>10$, $\mathbb{D}_3^{+}$ increases the counts of lags $\{1,2,3\}$. From the above analysis, this proof is finalized.

Compared with NA, OHNA-I exhibits lower initial weight function values, indicating reduced mutual coupling. However, as shown in (16), these values increase with the number of sensors exacerbating coupling and potentially reducing the accuracy of DOA estimation. To mitigate this effect and increase the continuous uDOF, OHNA-II is introduced.

3.3. OHNA-II

Proposition 5. (OHNA-II Configuration): Assuming that the total number of sensors is $N\geq 14$, the OHNA-II configuration is represented by set $\mathbb{R}_{\text{OHNA-II}}$, as follows

$$\mathbb{R}_{\text{OHNA-II}}=\mathbb{R}_1'\cup\mathbb{R}_2'\cup\mathbb{R}_3'\cup\mathbb{R}_4' \tag{17}$$

$$\begin{cases} \mathbb{R}_1'=\{0,3,4\} \\ \mathbb{R}_2'=\left\{\ell_1'\left(M_1+1\right)+1 \middle| 1\leq \ell_1'\leq M_2\right\} \\ \mathbb{R}_3'=\{\left(M_1+1\right)\left(M_2+1\right)+5 \\ \qquad +\ell_2' | 0\leq \ell_2'\leq M_1-7\} \\ \mathbb{R}_4'=\{M_1-1, \left(M_1+1\right)M_2+3, \\ \qquad \left(M_1+1\right)\left(M_2+1\right)\} \end{cases} \tag{18}$$

To illustrate the development process of the OHNA-II, we present an example comprising 18 sensors, as shown in Figure 3. It is evident that OHNA-II generates consecutive segments ranging from -107 to 107, achieving 215 uDOFs.

Proposition 6. For OHNA-II with position set $\mathbb{R}_{\text{OHNA-II}}$, (a) the contiguous segment of DCA spans the symmetric interval $\langle -v-M_1+2, v+M_1-2\rangle$, where $v=(M_1+1)(M_2+1)$. (b) It achieves a total of $2(M_1+1)(M_2+1)+2M_1-3$ uDOFs.

Proof: (a) Similar to the proof of Proposition 3, Proposition 6 is verified by performing self-difference and cross-difference operations. The self-difference sets for $\mathbb{R}_2'$ and $\mathbb{R}_3'$ are given as:

$$\begin{cases} \overline{\mathbb{D}}_1^{+}=\{0,1,3,4\} \\ \overline{\mathbb{D}}_3^{+}=\langle 0,2\rangle \end{cases} \tag{19}$$

The cross-difference set of $\mathbb{R}_1'$ and $\mathbb{R}_2'$ is given by

$$\overline{\mathbb{D}}_{2,1}^{+}=\{\mu_1\left(M_1+1\right)-3, \mu_1\left(M_1+1\right)-2, \mu_1\left(M_1+1\right) +1|1\leq\mu_1\leq M_2\} \tag{20}$$

The cross-difference sets between $\mathbb{R}_4'$ and $\mathbb{R}_2'$, and between $\mathbb{R}_4'$ and $\mathbb{R}_3'$ are defined as

$$\begin{cases} \overline{\mathbb{D}}_{4,2}^{+}=\{2, \mu_1\left(M_1+1\right)-1, \mu_3\left(M_1+1\right) \\ \qquad +2|1\leq\mu_1\leq M_2, 1\leq\mu_3\leq M_2-1\} \\ \overline{\mathbb{D}}_{4,3}^{-}=\{3+\mu_4, (M_1+1)+\mu_4, (M_1+1)(M_2+1) \\ \qquad -M_1+4+\mu_4|2\leq\mu_4\leq M_1-5\} \end{cases} \tag{21}$$

Combining (19) and (21), we derive the continuous range: $\langle 0, M_1\rangle$.

TABLE 2. Relationship between the number of sensors and uDOFs for different sparse arrays.

Array	Sensor Number	uDOFs
OHNA-I	odd: $N_1 = N/2, N_2 = N/2, N \geq 16$ even: $N_1 = (N-1)/2, N_2 = (N+1)/2, N \geq 16$	$(N+1)^2/2 + N + 6$ $N^2/2 + 2N + 7$
OHNA-II	odd: $N_1 = N/2, N_2 = N/2, N \geq 16$ even: $N_1 = (N-1)/2, N_2 = (N+1)/2, N \geq 16$	$N^2/2 + 3N - 5/2$ $N^2/2 + 3N - 1$
GAMSNA-I[13]	odd: $N_1 = 3, N_2 = (N+1)/2, N_3 = 1, N_4 = (N+1)/2 - 5, N \geq 12$ even: $N_1 = 3, N_2 = N/2, N_3 = 1, N_4 = N/2 - 4, N \geq 12$	$(N^2-1)/2 + N + 6$ $N^2/2 + N + 5$
GAMSNA-II[13]	odd: $N_1 = 3, N_2 = (N+1)/2, N_3 = 1, N_4 = \lceil (N+1)/4 - 5/2 \rceil,$ $N_5 = (N+1)/2 - 5 - N_4, N \geq 14$ even: $N_1 = 3, N_2 = N/2, N_3 = 1, N_4 = \lceil N/4 - 2 \rceil,$ $N_5 = N/2 - 4 - N_4, N \geq 14$	$(N^2-1)/2 + N + 6$ $N^2/2 + N + 5$
ANAI-1[10]	odd: $N_1 = N/2, N_2 = N/2$ even: $N_1 = (N-1)/2, N_2 = (N+1)/2$	$2N_2(N_1+1) + 2\lceil (N_1+1)/2 \rceil - 1$
ANAI-2[10]	odd: $N_1 = N/2, N_2 = N/2$ even: $N_1 = (N-1)/2, N_2 = (N+1)/2$	$2N_2(N_1+1) + 2N_1 - 5$
NA-CADiS[7]	$N_1 = (N+2)/2, N_2 = N/2$	$2N_1N_2 + 1$
NA-TS[12]	odd: $N_1 = (N - 2N_3 - 1)/2, N_2 = (N+1)/2, 1 \leq N_3 < (N-1)/2$ even: $N_1 = (N - 2N_3)/2, N_2 = N/2, 1 \leq N_3 < N/2$	$N^2/2 + 2N - 2N_3 - 3/2$ $N^2/2 + 2N - 2N_3 - 1$
NA[5]	odd: $N_1 = N/2, N_2 = N/2$ even: $N_1 = (N-1)/2, N_2 = (N+1)/2$	$2N_2(N_1+1) - 1$
ePCA[9]	odd: $N_1 = (3N+7)/12, N = 2N_1 + N_2 - 1$ even: $N_1 = (N+3)/4, N = 2N_1 + N_2 - 1$	$4N_1N_2 + 6N_1 - 2\lfloor N_1/2 \rfloor N_1 - 1$

The self-difference set of $\mathbb{R}_2^{'}$ is given by

$$\overline{\mathbb{D}}_2^{+} = \{\mu_3 (M_1 + 1) \,|\, 1 \leq \mu_3 \leq M_2 - 1\} \tag{22}$$

The cross-difference sets $\overline{\mathbb{D}}_{3,2}^{+}$ and $\overline{\mathbb{D}}_{4,2}^{-}$ are given by

$$\begin{cases} \overline{\mathbb{D}}_{3,2}^{+} = \{\mu_1 (M_1 + 1) + 4, \mu_1 (M_1 + 1) + 5, \\ \qquad \mu_1 (M_1 + 1) - 3 + M_1 \,|\, 1 \leq \mu_1 \leq M_2\} \\ \overline{\mathbb{D}}_{4,2}^{-} = \{\mu_1 (M_1 + 1) + 2 - M_1 \,|\, 1 \leq \mu_1 \leq M_2\} \end{cases} \tag{23}$$

Then, the range $\langle (M_1 + 1), M_2(M_1 + 1) - 1 \rangle$ is obtained.

For $\mathbb{R}_1^{'}$ and $\mathbb{R}_4^{'}$, the cross-difference set $\overline{\mathbb{D}}_{4,1}^{+}$ and self-difference set $\overline{\mathbb{D}}_4^{+}$ are given as follows

$$\begin{cases} \overline{\mathbb{D}}_{4,1}^{+} = \{M_1 - 5, M_1 - 4, M_1 + 1, M_2 (M_1 + 1) \\ \qquad -1, M_2 (M_1 + 1), M_2 (M_1 + 1) + 3\} \cup \\ \qquad \{(M_1 + 1)(M_2 + 1) - 4, (M_1 + 1) \\ \qquad (M_2 + 1) - 3, (M_1 + 1)(M_2 + 1)\} \\ \overline{\mathbb{D}}_4^{+} = \{0, M_1 - 2, M_2 (M_1 + 1) + 4 - M_1, \\ \qquad (M_1 + 1)(M_2 + 1) + 1 - M_1\} \end{cases} \tag{24}$$

For $\mathbb{R}_1^{'}$ and $\mathbb{R}_3^{'}$, the cross-difference set yields

$$\overline{\mathbb{D}}_{3,1}^{+} = \{\mu_2 + (M_1 + 1)(M_2 + 1) \,|\, 1 \leq \mu_2 \leq M_1 - 2\} \tag{25}$$

According to (24) and (25), $\overline{\mathbb{D}}_{4,1}^{+}$ contains $M_2(M_1 + 1)$, $M_2(M_1 + 1) + 3$ and $(M_1 + 1)(M_2 + 1)$; $\overline{\mathbb{D}}_4^{+}$ contains $(M_1 + 1)(M_2 + 1) - M_1 + 1$; $\overline{\mathbb{D}}_{3,1}^{+}$ contains $\langle (M_1 + 1)(M_2 + 1) + 1, (M_1 + 1)(M_2 + 1) + M_1 - 2 \rangle$.

Additionally, $\overline{\mathbb{D}}_{2,1}^{+}$ contains $M_2(M_1 + 1) + 1$; $\overline{\mathbb{D}}_{3,2}^{+}$ contains $\langle M_2(M_1 + 1) + 4, M_2(M_1 + 1) + M_1 - 3 \rangle$; $\overline{\mathbb{D}}_{4,3}$ contains $\langle (M_1 + 1)(M_2 + 1) - M_1 + 6, (M_1 + 1)(M_2 + 1) - 1 \rangle$. Thus, this proof is finalized.

(b) According to (20)–(25), the DCA of OHNA-II is free of holes. Taking into account the contributions of all subarrays within the negative portion of $\mathbb{D}$, the unique uDOFs is $2(M_1 + 1)(M_2 + 1) + 2M_1 - 3$.

Proposition 7. Given a particular P, the weight functions $w(\gamma)$ $(\gamma = 1, 2, 3)$ can be expressed

$$\begin{cases} w(1) = M_1 - 6, & M_1 \geq 7 \\ w(2) = \begin{cases} 2, & M_1 = 7 \\ M_1 - 7, & M_1 > 7 \end{cases} \\ w(3) = \begin{cases} 3, & M_1 = 7, 8 \\ M_1 - 7, & M_1 \geq 9 \end{cases} \end{cases} \tag{26}$$

Following from (16), the proof of Proposition 7 is omitted. A comparison between (16) and (26) shows that OHNA-II has a lower MC level than OHNA-I, which leads to its superior overall performance. Compared with OHNA-I, OHNA-II exhibits superior MC suppression performance. As sensors' count in-

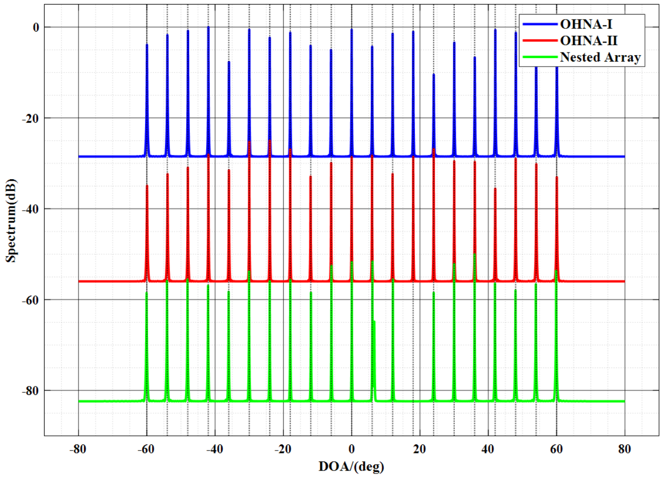

FIGURE 4. MUSIC spectrum of three nested arrays for 21 signals.

TABLE 3. Comparison of uDOFs across different array configurations under a fixed sensor count.

Array	Sensor Count				
	20	40	60	80	100
OHNA-II	259	919	1979	3439	5299
OHNA-I	247	887	1927	3367	5207
GAMSNA-I	225	845	1865	3285	5105
GAMSNA-II	225	845	1865	3285	5105
ANAI-1	231	861	1891	3321	5151
ANAI-2	235	875	1915	3355	5195
NA-CADiS	221	841	1861	3281	5101
NA	219	839	1859	3279	5099
NA-TS	223	843	1863	3283	5103
ePCA	197	711	1487	2621	3977

creases, the performance gap between these configurations becomes increasingly pronounced.

Table 2 presents a comparative summary of the uDOF expressions and sensor distributions under different sparse array frameworks, where N_l represents the number of subarrays. Table 3 provides a comparative assessment of the attainable uDOF across ten sparse array topologies as the number of physical sensors increases from 20 to 100 in steps of 20. Among the compared structures, OHNA-II achieves the most substantial growth in uDOF with increasing sensor count, which systematically fills vacant positions in the difference co-array, thereby enhancing the effective utilization of the available spatial DOF.

4. NUMERICAL SIMULATIONS

The performance of the proposed OHNA configurations is evaluated by comparing them to other well-known array architectures. DOA estimation for all arrays is performed using spatial smoothing-based subspace algorithms, with performance quantified by the root mean square error (RMSE).

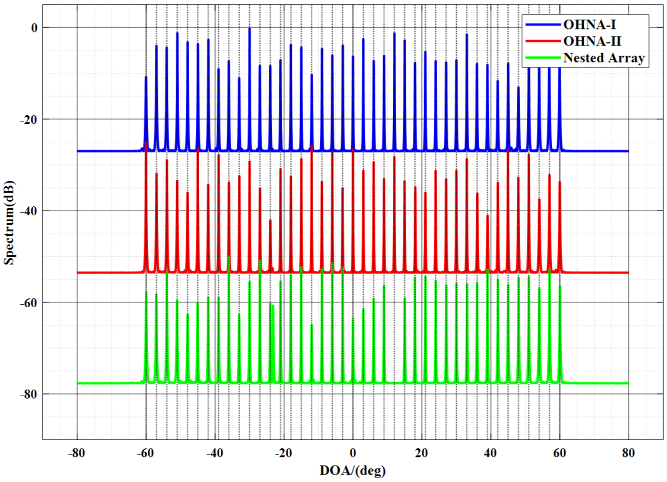

FIGURE 5. MUSIC spectrum of three nested arrays for 31 signals.

Definition 6. (Spatial efficiency): Spatial efficiency quantifies the capability of a sparse array to generate uDOFs, defined as

$$\alpha = \frac{N^2}{\text{card}\left\{\text{uDOFs}\right\}} \tag{27}$$

A smaller α corresponds to a larger number of uDOFs.

4.1. Comparison of DOA Spectrum

Firstly, we compare the DOA spectrum estimation performance of three nested array configurations under a relatively large sensor scale. The total number of sensors is set to 32, with a signal-to-noise ratio (SNR) of 0 dB. An extended covariance matrix is estimated using 300 snapshots. The Multiple Signal Classification (MUSIC) algorithm scans from -90° to 90° with a step size of 0.1°. Figures 4–6 display the MUSIC spectra for the three arrays when 21, 31, and 41 signals are uniformly distributed between -60° and 60°. From Figure 4, it is evident that all three arrays can successfully resolve 21 signals. However, as observed in Figures 5 and 6, a portion of spectral peaks overlap in the conventional NA, whereas both proposed OHNA-I and OHNA-II maintain clear discrimination of all 31 signals.

Secondly, we incorporate the effect of mutual coupling among array elements under the aforementioned conditions. Figure 7 shows the MUSIC spectra for the three arrays in the presence of 31 signals. The results indicate that the proposed OHNA-I structure is affected by mutual coupling, leading to noticeable spectral leakage in its MUSIC spectrum. In contrast, OHNA-II retains a high-resolution capability without significant peak overlap or leakage.

4.2. Sensitivity Analysis of MC and Comparative Evaluation

Table 4 presents the performance comparison results of ten array configurations in the presence of MC. We employed the MC model provided in Section 2.2, with a coupling coefficient of $m_1 = 0.3e^{j\pi/3}$. The other coefficients are set to $m_a = m_1 e^{-j(\rho-1)\pi/8}/\rho\,(2 \leq \rho \leq 100)$ with $B = 100$.

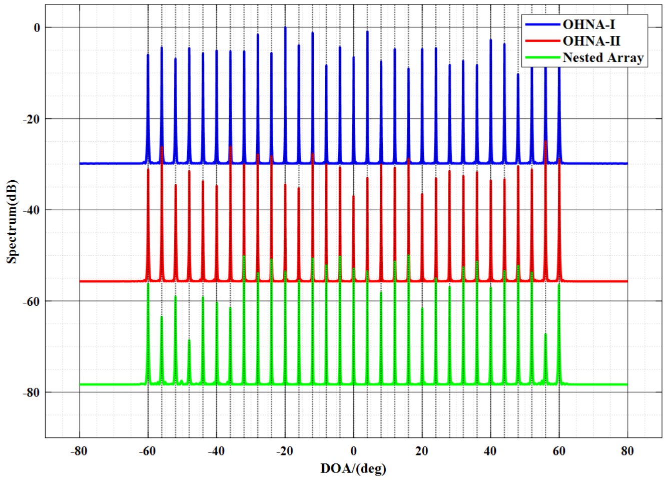

FIGURE 6. MUSIC spectrum of three nested arrays for 41 signals.

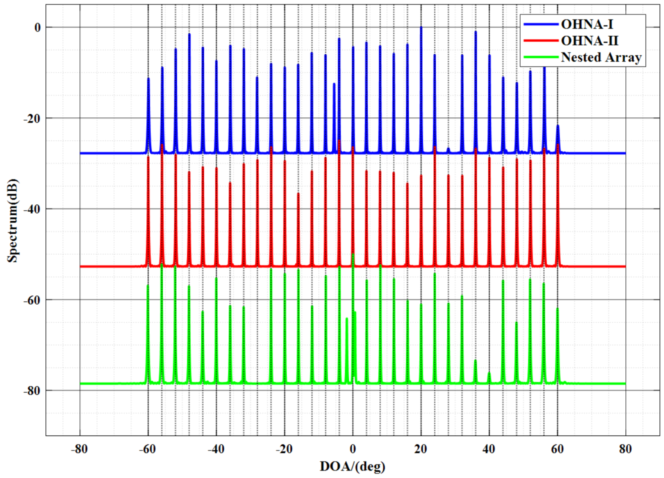

FIGURE 7. MUSIC spectrum of three nested arrays for 31 signals in the presence MC.

TABLE 4. Comparison of weight function and mutual coupling in sparse arrays with 18 sensors, where the MC model is provided in Section 4.2.

	OHNA-II	OHNA-I	GAMSNA-I	GAMSNA-II	NA-TS
$w(\gamma)$	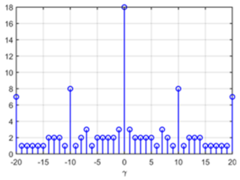	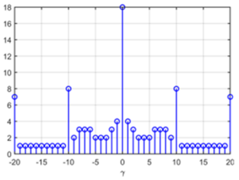	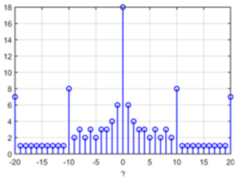	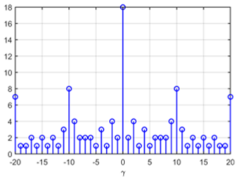	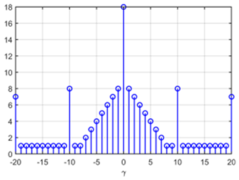
C	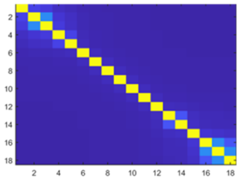	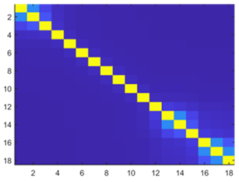	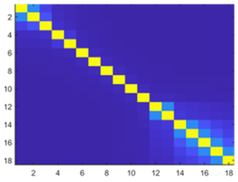	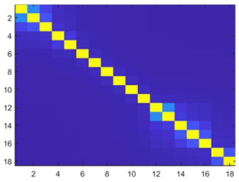	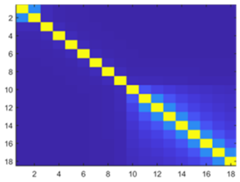
(R)	0.2023	0.2300	0.2700	0.1898	0.3178
	ANAI-1	ANAI-2	NA	NA-CADiS	ePCA
$w(\gamma)$	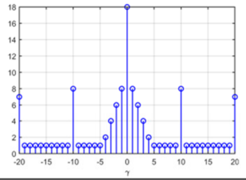	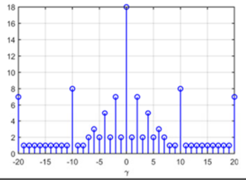	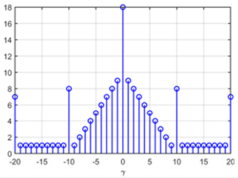	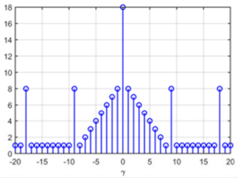	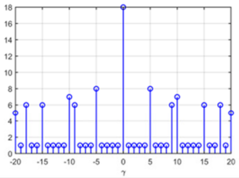
C	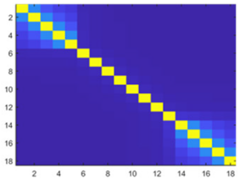	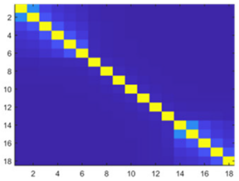	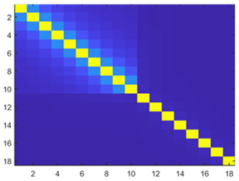	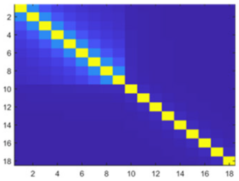	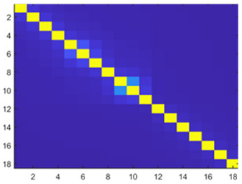
(R)	0.3066	0.2121	0.3364	0.3181	0.1435

In the first case, we form each array with 18 sensors. Then, weight functions of the arrays are displayed in the second row; the MC matrices for each array are in the third row; and the MC leakage is in the last row. As noted in Section 2.2, MC leakage ranges from 0 to 1, with lower values being ideal, and the first three weight values play a significant role in determining the MC leakage of an array. To present the comparison results more intuitively, we employ a gradient color map to represent the MC matrix, where lighter colors indicate stronger mutual coupling.

From Table 4, it can be seen that all arrays exhibit the weakest performance due to the highest MC leakage values. ePCA demonstrates optimal MC suppression with the lowest leakage. The OHNAs configuration perform intermediately, with

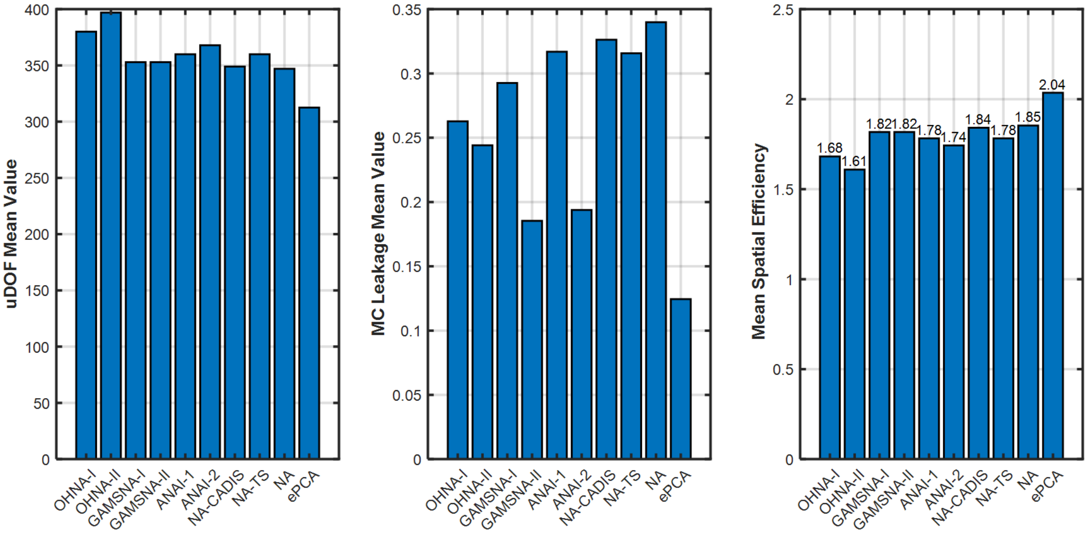

FIGURE 8. Performance comparison histogram of ten sparse array configurations.

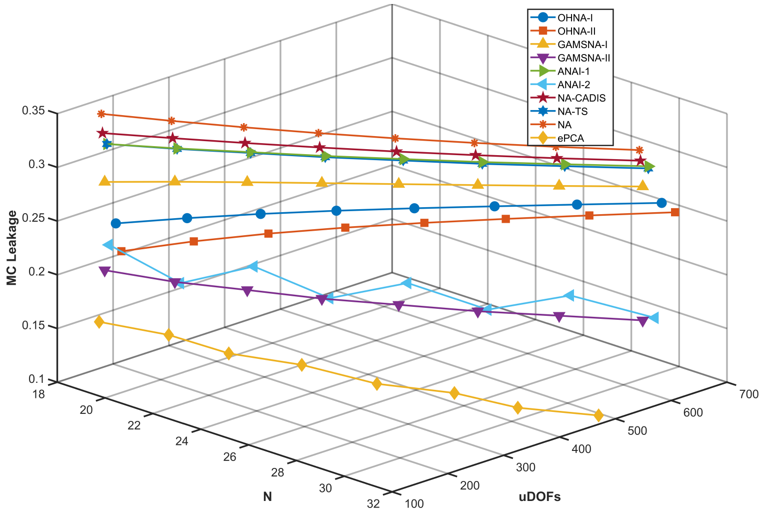

FIGURE 9. Three-dimensional representation of the relationship between sensor count, uDOFs, and MC leakage for different array architectures.

OHNA-II exhibiting superior MC suppression compared to OHNA-I.

Then, to clearly evaluate the robustness of the proposed OHNAs configuration and validate the rationale behind the evolution from OHNA-I to OHNA-II, Figure 8 visually illustrates the performance differences among these sparse arrays as the number of sensors increases from 18 to 32. Histogram 1 shows the mean uDOFs for each array, histogram 2 the mean MC leakage for each array, and histogram 3 the mean spatial efficiency for each array. From Figure 8, OHNA-II outperforms OHNA-I across all metrics, validating the rationale behind its evolution. Compared to OHNA-I, OHNA-II significantly reduces MC leakage through structural optimization while maintaining high uDOFs and spatial efficiency across all arrays, demonstrating its robust advantages in practical applications.

Figure 9 clearly illustrates the three-dimensional relationship among sensor count, uDOFs, and MC leakage across different array configurations. While most arrays cluster in regions favoring either high uDOFs or low mutual coupling, the proposed OHNA variants consistently achieve both. Notably, OHNA-II strikes an optimal balance between maximizing uDOFs and minimizing MC, outperforming other arrays.

4.3. Estimation Accuracy

The RMSE is defined as

$$\mathrm{RMSE}=\sqrt{\frac{1}{JK}\sum_{j=1}^{J}\sum_{k=1}^{K}(\widehat{\theta}_k(j)-\theta_k)^2} \tag{28}$$

where J is the number of Monte Carlo trails, set to 300 in this section, and $\widehat{\theta}_k(j)$ is the estimated angle for jth ($j=1,2,...,300$) trail.

For the RMSE analysis, all arrays are configured with 18 sensors. The spatially smoothed MUSIC algorithm [21] is employed to estimate the arrival directions of signal sources. We analyze RMSE under two scenarios: one disregarding the MC between sensors, and the other accounting for mutual coupling.

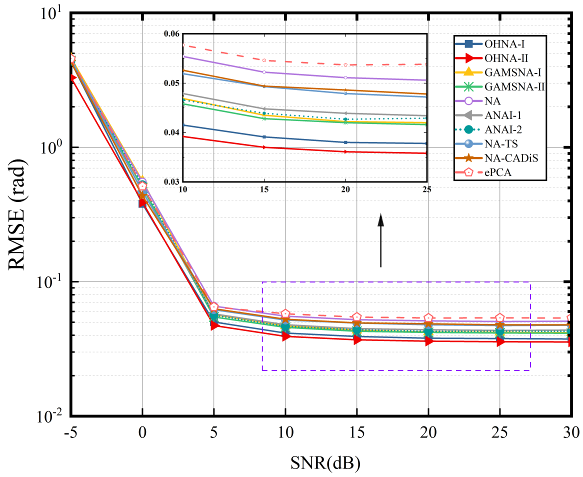

FIGURE 10. RMSE against SNR for ten arrays without MC.

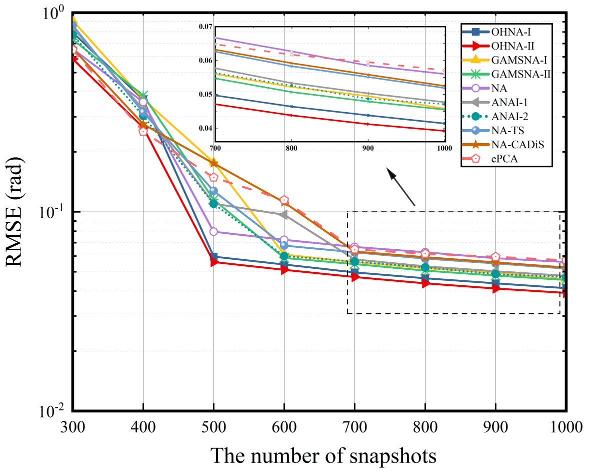

FIGURE 11. RMSE against snapshots for ten arrays without MC.

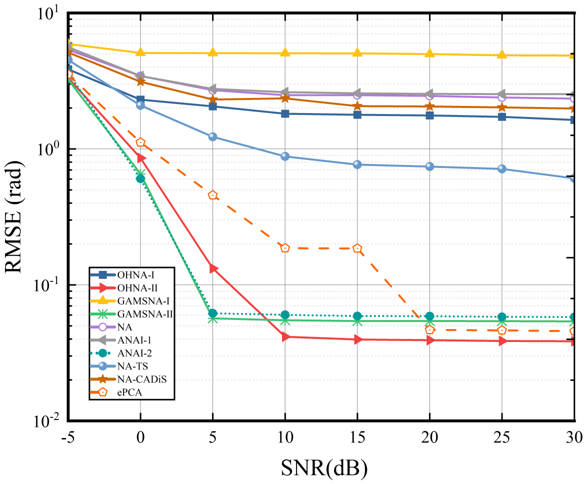

FIGURE 12. RMSE against SNR for ten arrays considering MC.

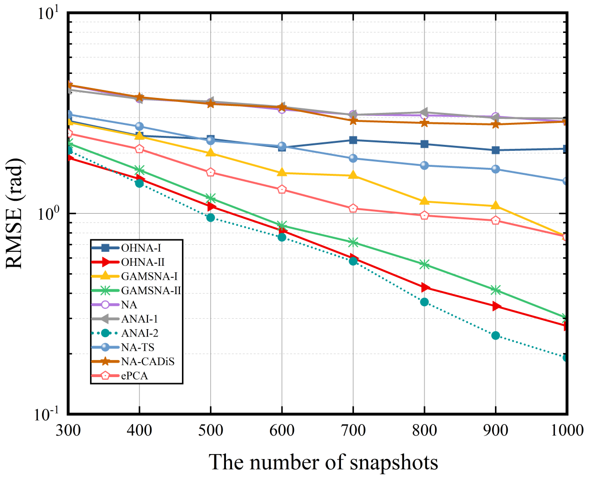

FIGURE 13. RMSE against snapshots for ten arrays considering MC.

The simulation considered 31 signal sources uniformly distributed within the range from -60° to 60°.

Without considering MC, we respectively examine the RMSE performance of each array under different SNRs and varying snapshots. Figure 10 plots the RMSE versus SNR with $K = 500$. It can be seen that all arrays show rapid RMSE reduction with increasing SNR, stabilizing above 5 dB. Notably, OHNA-II maintains the lowest RMSE from 10 to 25 dB, benefiting from its superior uDOFs. Figure 11 plots the RMSE versus snapshots with SNR $= 0$ dB. The results indicate a steady improvement in estimation accuracy as more snapshots are collected, with the RMSE progressively decreasing. Arrays with more uDOFs exhibit greater stability and outperform those with fewer uDOFs, especially at higher snapshot numbers.

When considering mutual coupling, we assume the MC coefficient $m_1 = 0.3e^{j\pi/3}$, $B = 100$, and $m_a = m_1 e^{-j(\rho-1)\pi/8}/\rho\,(2 \leq \rho \leq 100)$. Figure 12 depicts the RMSE versus SNR with $K = 500$. It can be observed that GAMSNA-I and OHNA-I exhibit significant increases in RMSE, indicating pronounced degradation in DOA estimation performance. In contrast, OHNA-II demonstrates superior robustness, with only minimal accuracy loss, owing to its extended continuous segments. Figure 13 plots the RMSE versus snapshots with SNR $= 0$ dB. It can be observed that the mutual coupling effects degrade the RMSM performance of OHNA-I. Among the compared arrays, the NA suffers most from mutual coupling, while OHNA-II performs relatively better. This advantage is primarily attributed to its larger number of uDOFs, which supports more stable DOA estimation as the number of sensors increases. Figure 14 compares the trends of RMSE with respect to the mutual coupling coefficient. The proposed OHNA configurations achieve the lowest RMSE when $|m_1| = 0$, and as the coupling strength increases, OHNA-II maintains a favorable trade-off between uDOFs and mutual coupling effects.

Subsequently, to further analyze the array performance, we compared the RMSE under different numbers of sources with $K = 500$ and SNR $= 0$ dB. As shown in Figure 15, the RMSE of all arrays increases with the number of sources. Among them, ePCA consistently exhibits the highest RMSE; OHNA-II maintains the lowest RMSE; and OHNA-I lies between the

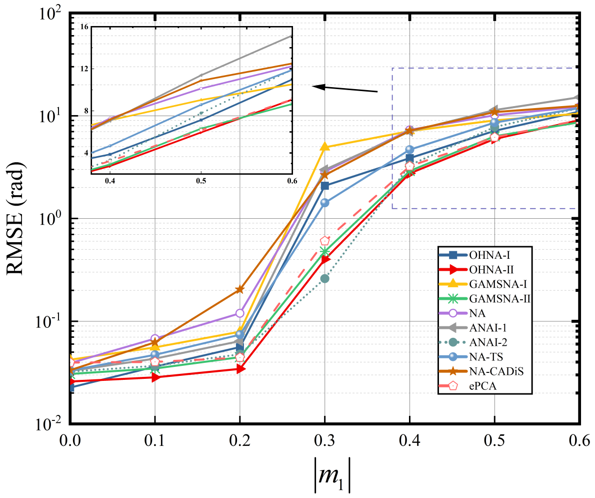

FIGURE 14. RMSE against MC coefficient for ten arrays.

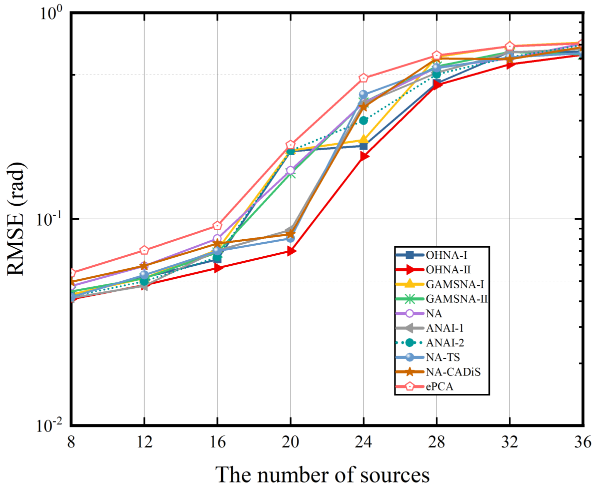

FIGURE 15. RMSE against sources for ten arrays without MC.

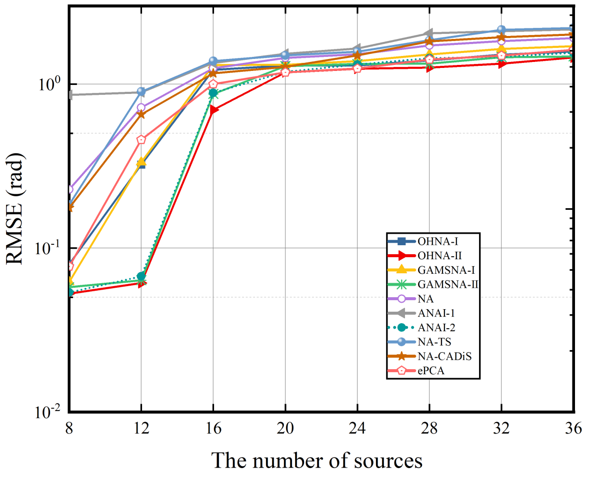

FIGURE 16. RMSE against sources for ten arrays considering MC.

two. As shown in Figure 16, when mutual coupling is present, ANAI-I is affected most, and OHNA-I also experiences performance degradation. However, OHNA-II remains at the lowest RMSE level consistently, indicating that the proposed OHNA-II configuration demonstrates superior robustness to mutual coupling compared with the other arrays.

5. CONCLUSION

This paper revisits the signal model of sparse arrays and proposes an OHNA-I configuration that is capable of generating a substantial number of uDOFs. Analytical expressions for the sensor positions, uDOFs, and weight functions are derived. To further expand the effective aperture, increase uDOFs, and mitigate mutual coupling, a new OHNA-II configuration is introduced through subarray translation. Extensive simulations validate that the proposed arrays significantly enhance uDOFs, mutual coupling suppression, and DOA estimation accuracy. Subsequent research focuses on refining the array configuration to further minimize coupling effects and improve the robustness and precision of DOA estimation.

ACKNOWLEDGEMENT

This work is supported in part by the Shaanxi Qinchuangyuan “Scientists + Engineers” Team Construction Project under Grant 2024QCY-KXJ-168, and in part by the Project Supported by Natural Science Basic Research Plan in Shaanxi Province of China under Grant 2023-JC-YB-484.

REFERENCES

[1] Ling, Y., H. Gao, S. Zhou, L. Yang, and F. Ren, “Robust sparse Bayesian learning-based off-grid DOA estimation method for vehicle localization,” *Sensors*, Vol. 20, No. 1, 302, Jan. 2020.

[2] Sun, H., Y. Liu, A. Al-Tahmeesschi, A. Nag, M. Soleimanpour, B. Canberk, H. Arslan, and H. Ahmadi, “Advancing 6G: Survey for explainable AI on communications and network slicing,” *IEEE Open Journal of The Communications Society*, Vol. 6, 1372–1412, 2025.

[3] Shi, J., Z. Yang, and Y. Liu, “On parameter identifiability of diversity-smoothing-based MIMO radar,” *IEEE Transactions on Aerospace and Electronic Systems*, Vol. 58, No. 3, 1660–1675, Jun. 2022.

[4] Moffet, A., “Minimum-redundancy linear arrays,” *IEEE Transactions on Antennas and Propagation*, Vol. 16, No. 2, 172–175, Mar. 1968.

[5] Pal, P. and P. P. Vaidyanathan, “Nested arrays: A novel approach to array processing with enhanced degrees of freedom,” *IEEE Transactions on Signal Processing*, Vol. 58, No. 8, 4167–4181, Aug. 2010.

[6] Vaidyanathan, P. P. and P. Pal, “Sparse sensing with co-prime samplers and arrays,” *IEEE Transactions on Signal Processing*, Vol. 59, No. 2, 573–586, Feb. 2011.

[7] Qin, S., Y. D. Zhang, and M. G. Amin, “Generalized coprime array configurations for direction-of-arrival estimation,” *IEEE Transactions on Signal Processing*, Vol. 63, No. 6, 1377–1390, Mar. 2015.

[8] Raza, A., W. Liu, and Q. Shen, “Thinned coprime array for second-order difference co-array generation with reduced mutual coupling,” *IEEE Transactions on Signal Processing*, Vol. 67, No. 8, 2052–2065, Apr. 2019.

[9] Zheng, W., X. Zhang, Y. Wang, J. Shen, and B. Champagne, “Padded coprime arrays for improved DOA estimation: Exploit-

ing hole representation and filling strategies," *IEEE Transactions on Signal Processing*, Vol. 68, 4597–4611, 2020.

[10] Liu, J., Y. Zhang, Y. Lu, S. Ren, and S. Cao, "Augmented nested arrays with enhanced DOF and reduced mutual coupling," *IEEE Transactions on Signal Processing*, Vol. 65, No. 21, 5549–5563, Nov. 2017.

[11] Shaalan, A. M. A., J. Du, and Y.-H. Tu, "Dilated nested arrays with more degrees of freedom (DOFs) and less mutual coupling — Part I: The fundamental geometry," *IEEE Transactions on Signal Processing*, Vol. 70, 2518–2531, 2022.

[12] Zhang, Y., G. Hu, H. Zhou, J. Bai, C. Zhan, and S. Guo, "Hole-free nested array with three sub-ULAs for direction of arrival estimation," *Sensors*, Vol. 23, No. 11, 5214, 2023.

[13] Wei, S., G. Zhu, and Y. Su, "A novel sparse array configuration for direction of arrival estimation with increased uniform degrees of freedom and reduced mutual coupling," *Sensors*, Vol. 24, No. 3, 808, Jan. 2024.

[14] Wandale, S. and K. Ichige, "A generalized extended nested array design via maximum inter-element spacing criterion," *IEEE Signal Processing Letters*, Vol. 30, 31–35, 2023.

[15] Wang, X., L. Zhao, and Y. Jiang, "Super augmented nested arrays: A new sparse array for improved DOA estimation accuracy," *IEEE Signal Processing Letters*, Vol. 31, 26–30, 2024.

[16] Friedlander, B. and A. J. Weiss, "Direction finding in the presence of mutual coupling," *IEEE Transactions on Antennas and Propagation*, Vol. 39, No. 3, 273–284, Mar. 1991.

[17] Liu, C.-L. and P. P. Vaidyanathan, "Super nested arrays: Linear sparse arrays with reduced mutual coupling — Part I: Fundamentals," *IEEE Transactions on Signal Processing*, Vol. 64, No. 15, 3997–4012, Aug. 2016.

[18] Wang, M., X. Ma, S. Yan, and C. Hao, "An autocalibration algorithm for uniform circular array with unknown mutual coupling," *IEEE Antennas and Wireless Propagation Letters*, Vol. 15, 12–15, 2015.

[19] Chen, H., H. Lin, W. Liu, Q. Wang, Q. Shen, and G. Wang, "Augmented multi-subarray dilated nested array with enhanced degrees of freedom and reduced mutual coupling," *IEEE Transactions on Signal Processing*, Vol. 72, 1387–1399, 2024.

[20] Lai, X., X. Zhang, W. Zheng, J. Li, and F. Zhou, "Fragmented coprime arrays with optimal inter subarray spacing for DOA estimation: Increased DOF and reduced mutual coupling," *Signal Processing*, Vol. 215, 109273, Feb. 2024.

[21] Qi, C., Y. Wang, Y. Zhang, and Y. Han, "Spatial difference smoothing for DOA estimation of coherent signals," *IEEE Signal Processing Letters*, Vol. 12, No. 11, 800–802, Nov. 2005.